Synthesis of an Al-based Al-Cr-Co-Ce alloy by mechanical alloying and its thermal stability

S. Mula, S. Ghosh and S. K. Pabi*

Department of Metallurgical and Materials Engineering, Indian Institute of Technology, Kharagpur, India, Pin-721 302

*Author for correspondence: Email: skpabi@metal.iitkgp.ernet.in
Phone: 91-3222-283272, Fax: 91-3222-282280

Abstract

Amorphous and nanocrystalline phases generated in an elemental blend of $Al_{94.5}Cr_3Co_{1.5}Ce_1$ composition (at.%) in the course of mechanical alloying (MA) have been investigated by X-ray diffraction (XRD), transmission electron microscopy (TEM), scanning electron microscopy (SEM) and differential scanning calorimeter (DSC). It has been reported that rapid solidification processing (RSP) of the same composition generates a finely mixed unique structure consisting of nanoscale icosahedral (I) particles surrounded by a thin Al phase [1]. In contrast, MA of $Al_{94.5}Cr_3Co_{1.5}Ce_1$ composition carried out in the present study shows the formation of Al-based solid solutions along with partial

amorphisation. It emerges that during MA a wide difference in the atomic size of the alloying elements in solid solution plays a pivotal role in the amorphous phase formation. The possible causes of the difference in microstructure generated by MA and RSP have been discussed. The thermal stability of the mechanically alloyed product has also been investigated by a differential scanning calorimeter (DSC) and XRD.

Key words: Amorphisation, Mechanical Alloying, Nanocrystalline, X-ray Diffraction, Transmission Electron Microscopy, Thermal Stability.

Introduction

Development of Al based bulk metallic glass or composite with a high specific strength is always of great importance to the transportation and aviation industry. Non-equilibrium processing of materials by mechanical alloying (MA) through high-energy ball milling or rapid solidification processing (RSP) has attracted wide attention in recent times due to the possibility of producing better and improved high strength structural materials than those possible by the conventional methods [2]. Annealing of bulk amorphous alloys at an appropriate temperature can form a dispersion of nanocrystalline intermetallic phases in the mechanically alloyed amorphous matrix precursors [3-6]. The strength of light weight aluminum alloys could be significantly enhanced from about 600 MPa in age hardened condition to over 1500 MPa in the rapidly quenched amorphous alloys or nanocomposites [7]. The strength of

nanocrystalline solid solutions depends on both solid solution hardening and grain boundary hardening [8].

The formation of solid solution and amorphous phases by MA technique was investigated by many researchers [9-12]. Tsurui *et al.* [13] studied the Al based amorphous phase formation with a blend composition of $Al_{85}Co_{15}$ by mechanical milling of pre-alloyed $Al_{13}Co_4$ and Al powders, which could not be prepared by MA of an elemental blend of Al and Co powders. The formation of supersaturated solid solutions by MA was reported by Huang *et al.* [14] in their research work. The microscopic mechanisms which, during high energy ball milling of metallic articles, induce a variety of solid state reactions like alloying, order-disorder transformations, amorphisation and other phase changes are not well understood [15]. The three major contributing factors to glass formation are atomic size mismatch, high negative heat of mixing, and multicomponent alloy system [16]. Rao [17] postulated that an alloy with the smallest possible molar volume is the one that is most prone to glass formation. Egami [18] discussed the theory of topological instability of the local atomic structure due to atomic size difference and its concentration to explain the solid state amorphisation.

The thermodynamic and kinetic factors affecting amorphisation during solid-state reaction annealing of pure metal-metal multilayer and of mixtures of metal

powders during co-deformation (MA) were reported by Yavari *et al.* [19]. The amorphous and nanocrystalline structures generated in quaternary systems containing Al, mischmetal (Mm) and late transition metals (TM) were analyzed by Latuch *et al*. [20]. One of the distinct features possessed by nanocrystalline materials prepared by MA is the presence of a high level of internal stresses [21]. While the determination of the lattice microstrain in the mechanically alloyed nanocrystalline products often relies on the x-ray diffraction (XRD) alone, the grain size is usually estimated from the XRD data and corroborated independently with the TEM measurements [21, 22].

The RSP of $Al_{94.5}Cr_3Co_{1.5}Ce_1$ composition (in atom %) was reported to generate a finely mixed unique structure consisting of nanoscale icosahedral (I) particles surrounded by a thin layer of Al phase [1]. These microstructures are the result of freezing-in of the solutes and thermal disorder. On the other hand, MA generates a nonequilibrium structure by introducing extensive mechanical disorder, crystallite size refinement and sometimes by inducing excess solid solubility. Therefore, in the present investigation it is intended to examine the phase evolution during MA of the same alloy, *i.e.,* $Al_{94.5}Cr_3Co_{1.5}Ce_{1,}$ and also to determine its thermal stability. The outcome has been discussed in the light of a mechanically induced alloying mechanism.

Experimental

Powder blends of elemental Al, Cr, Co and Ce (purity >99.5 wt %, particle size <70 μm) having a nominal composition of $Al_{94.5}Cr_3Co_{1.5}Ce_1$ (in at %) were ball milled in a high energy Fritsch Pulverisette-5 planetary ball mill having cemented carbide grinding media, at a mill speed of 300 *r.p.m.* and a ball to powder ratio of 10:1, using toluene as the process control agent. The identity and phase evolution at different stages of MA were studied by XRD analysis using the Co-Kα radiation (λ =0.1789 nm) in a Philip's X'pert PRO high-resolution x-ray diffractometer. The refined values of lattice parameter (*a*) were calculated from the peak positions in the XRD pattern by extrapolation of *a* against ($\cos^2\theta$ /sinθ) plot to cosθ = 0 [23]. The average grain size of Al-rich solid solution was determined from the broadening of a Al_{111} reflection after K-α_2 stripping by the Philips X'pert Plus software and using the Voigt method [24], which allowed judicious elimination of the contribution due to instrumental and strain effects on the observed peak broadening. For the overlapping peaks, the full width at half intensity maximum and the true Bragg angle (2θ) were determined by an appropriate deconvolution exercise. The thermal stability of the mechanically alloyed product was characterized by a differential scanning calorimeter (DSC) (Perkin Elmer –Pyris Diamond) and XRD. The powder products were carefully wrapped up in a thin Al foil and then annealed at 200ºC for 2 h under a high purity argon (<10 ppm impurity) atmosphere. A JEOL JEM-2100 transmission electron microscope was employed for the determination of particle size and crystalline nature of the milled sample. A few samples were

examined by a JEOL JSM-840A scanning electron microscope (SEM) for the microstructural characterisation.

Results and Discussion

The SEM micrograph in Fig. 1(a) displays the layered structure of the coarse powder particles after 5 h of milling, while Fig. 1(b) evidences a substantial reduction in the particle size and uniformity of the composition of the particles after milling the $Al_{94.5}Cr_3Co_{1.5}Ce_1$ elemental blend for 30 h.

Fig. 2(a) shows the modulation of the XRD pattern of the same composition with the progress of MA. It is interesting to note that the intermetallic compounds of Al, Cr, Co and Ce, namely $Al_{13}Co_4$ and CeAlCo, formed during the early stage of milling, *i.e.*, 3 h to 15 h. However, on further milling these intermetallic compounds gradually disappeared (Fig. 2(a)). The enlarged XRD pattern after 60 h of MA of the same composition is presented separately in Fig. 2(b) for better illustration of the phase evolution after prolonged MA. Here, after 60 h of milling the structure appears to be substantially amorphous, as evidenced by the presence of an amorphous hump (Fig. 2(b)). The complicated nature of the ball milling process, as well as the complexity and sequence of dissolution of the alloying elements in the matrix during the MA process [25-29] are possibly responsible for the formation of intermetallic compounds in the early stage of milling. Here the dissolution of Cr, Co and Ce in the Al matrix, coupled with the structural defects induced by the MA process seem to promote partial

amorphisation. Nevertheless, it emerges from the present study, that the phases generated in $Al_{94.5}Cr_3Co_{1.5}Ce_1$ alloy by MA are quite different from those reported for the RSP of the same composition [1]

The analysis of the XRD patterns in Fig. 1(a) reveals that the crystallite size of Al initially decreases rapidly and then attains a nearly constant value of ~ 20 nm after 30 h of milling (Fig. 3). The TEM image of the powder milled for 60 h is displayed in Fig. 4. The average size of the particles is of the order of 40 nm, which corroborates well with the crystallite size of Al estimated from the XRD spectra. The electron diffraction pattern of 60 h milled powder in the inset of Fig. 4 shows a diffused halo due to the amorphous phase superimposed on the spotty pattern from the nanocrystalline Al phase. The TEM micrograph and the electron diffraction pattern clearly indicate that each nanoparticle is a nanocomposite after 60 h of MA. In an exhaustive review, Eckert [30] has demonstrated that it is very difficult to achieve complete amorphisation during MA of the alloys containing more than 80 at.% Al, and often the structure shows coexistence of an amorphous phase and the fcc Al-rich matrix with some intermetallic compound(s) [31-33]. The kinetic factors like the competition between amorphisation and crystallization, and the structural factors like the extent of crystallite size refinement and the stability of any intermetallic phase(s) formed during milling under continued deformation may have a decisive role in the amorphisation of Al-rich composition by MA.

Fig. 5 shows that the lattice microstrain (%) increases with milling time up to 60 h of MA, while Fig. 6 shows an increase in the lattice parameter of Al-rich solid solution (a_{Al}) after an initial decline in the $Al_{94.5}Cr_3Co_{1.5}Ce_1$ composition. The refined values of a_{Al} shows a gradual decrease till 18 h of milling, and thereafter it shows some increase up to 60 h of MA (Fig. 6). The atomic radii of Cr (0.1249nm) and Co (0.125nm) are very close to each other, and they are less than that of Al (0.14318nm). The atomic size differences in this case, however, is well within 15% of the atomic radius of Al [34], and hence in the light of the Hume-Rothery rules, the Cr and Co are expected to enter into the solid solution in Al during the early stage of MA. On the other hand, the increase in lattice parameter after MA for durations greater than 18 h may be attributed to the dissolution of Ce, which has a much larger atomic size (atomic radii 0.18244nm) compared to that of Al atoms, and the size difference exceeds 28% indicating its sparing solid solubility in Al.

In order to verify this view, the variation of crystallite size and a_{Al} during MA of a fully amorphous forming Al-rich composition recently reported by Das *et al.*, *i.e.,* $Al_{88}Ni_6Ti_6$ [28, 29], have been compared with those for the present alloy. The variations of crystallite size, lattice microstrain (%) and a_{Al} in a partially amorphous forming alloy, *i.e.,* $Al_{60}Ni_{20}Ti_{20,}$ with milling time were calculated from the experimental XRD data reported in [29], and the results are superimposed in Fig. 3, Fig. 5 and Fig. 6, respectively. The variation of lattice microstrain (%) of $Al_{88}Ni_6Ti_6$ alloy with milling time was also calculated from the

experimental XRD data reported in [28], and the results are superimposed in Fig. 5. The results in Fig. 3 and Fig. 5 demonstrate that the pattern of variations of crystallite size and lattice microstrain (%) with milling time in all the three Al-rich alloys are very similar up to 60 h of MA. But, the variation of lattice parameter of Al rich solid solution is much more pronounced in the case of $Al_{88}Ni_6Ti_6$ alloy (Fig. 6), which has also yielded a completely amorphous structure, compared to partial amorphisation in the $Al_{94.5}Cr_3Co_{1.5}Ce_1$ and $Al_{60}Ni_{20}Ti_{20}$ compositions under an identical condition of MA. Thus, Fig. 3 along with Fig. 5 indicate that the excess energy stored in the milled products in the form of crystallite size and lattice microstrain for all the three alloys are of the same order, and therefore these cannot account for the diversity in structure of the as-milled products in the three Al-rich alloys. On the other hand, calculations based on the Miedema's semi-empirical model extended to ternary system coupled with systematic experimentation by Das *et al.* [28] had earlier shown that the absolute values of enthalpies of amorphization ΔH^{amor} and mixing ΔH^{mix} are not the appropriate criteria for amorphization in the Al-Ni-Ti system. Therefore, Fig. 6 strongly suggests that a wide variation of a_{Al} in the course of MA by addition of the appropriate type and quantity of alloying elements can play an important role in the design of amorphous forming compositions. This view is in tune with the 'confusion principle' [16] and Egami's [18] criterion proposed earlier. Present results indicate that the atomic size diversity of the constituent elements and their concentration in the alloy, rather than the

energy stored in the form of lattice microstrain and internal/external surfaces possibly play a decisive role in the topological instability of the local atomic structure provoking the glass formation. Naturally, any portion of these alloying additions utilized in the formation of intermetallic compounds is not expected to contribute to the desired lattice parameter variation for amorphisation.

Fig. 7 shows the nature of thermal stability of the 60 h milled sample studied by DSC during heating at a rate of 5ºC min^{-1} up to 200ºC under a helium atmosphere. First an endothermic peak appears at around 100ºC depicting a small change of enthalpy, ΔH = 0.69 J/g, which is possibly associated with the evaporation of adsorbents (like moisture and/or toluene) from the milled product. Thereafter, two prominent exothermic peaks appear, one at ~148ºC (ΔH = -123 J/g) and the other at ~187ºC (ΔH = -296 J/g), which are apparently indicative of some transformation in the milled product. In order to get an insight into this event, the 60 h milled sample has been annealed at 200ºC for 2 h, and the XRD pattern of the annealed product shows a pronounced presence of the intermetallic compounds $Al_{13}Co_4$ and AlCo, as shown in Fig. 8. This strong tendency of forming intermetallic compounds at relatively low temperatures (148ºC and 187ºC) is not attractive for the consolidation of this nanostructure powders by pressure-less sintering. On the other hand, it has been reported that the amorphous structure of the same alloy, *i.e.,* $Al_{94.5}Cr_3Co_{1.5}Ce_1$, produced

by RSP could be maintained during annealing for 3.6 ks at 550ºC [35, 36]. The high thermal stability of this structure produced by RSP is completely in contrast with the inferior thermal stability of the mechanically alloyed nanostructured product of the same composition obtained in the present investigation.

Finally, it may be recalled that the unique mixed structure of nanoscale icosahedral (I) particles surrounded by a thin Al rich layer generated by RSP of the $Al_{94.5}Cr_3Co_{1.5}Ce_1$ composition is not reproduced by the present MA. This divergence can originate from the difference in the mechanisms of non-equilibrium phase formation in the two processing routes. In RSP all the alloying elements are in solution in the liquid prior to rapid solidification, and these along with the thermal disorder are frozen-in during solidification, while the sequence of dissolution of different alloying elements and the mechanical disorder induced by the MA process are likely to dictate the resultant phase evolution.

Conclusions

1. Prolonged (60 h) MA of the $Al_{94.5}Cr_3Co_{1.5}Ce_1$ composition has yielded partially amorphous structure, which is quite different from that reported

for the RSP of the same composition. This is possibly due to the difference in the sequence of phase formation and the nature of imperfections introduced in the two processes.

2. A wide variation in lattice parameter of the Al-rich solid solution caused by some suitable combination of the alloying additions (*e.g.* Cr, Co and Ce, or Ni and Ti) seems to play a pivotal role in the amorphisation during MA.
3. The thermal stability of the solid solution formed in the $Al_{94.5}Cr_3Co_{1.5}Ce_1$ alloy by MA is not quite attractive, because intermetallic compounds form during annealing at relatively low temperatures, *i.e.,* at 130-190ºC.

Acknowledgements

The work was sponsored by the Department of Science and Technology, Govt. of India through grant no. SR/S5/NM-91/2002 and the Defence Research and Development Organization, Govt. of India through grant no. ERIP/ER/0100169/M/01.

References

[1]. A. Inoue, Nanostructured Mater. 6 (1995) 53-64.

[2]. C. Suryanarayana, E. Ivanov, V.V. Boldyrev, Mater. Sci. Eng. A 304–306 (2001) 151-158.

[3]. A.P. Tsaip, T. Kamiyama, Y. Kawamura, A. Inoue, T. Masumotos, Acta Mater. 45 (1997) 1477-1487.

[4]. C.C. Koch, Mater. Sci. Eng. A 244 (1998) 39-48.

[5]. C. Suryanarayana, Prog. Mater. Sci. 46 (2001) 1-184.

[6]. M.S. El-Eskandarany, K. Aoki, K. Suzuki, Scripta Metall. Mater. 36 (1997) 1001-1009.

[7]. T. Masumoto, Mater. Sci. Eng. A 179-180(1994) 8-16.

[8]. T. D. Shen, C. C. Koch, Acta mater. 44 (1996) 753-761.

[9]. C. Gente, M.Oehring, R. Bormann, Phys. Rev. B 48 (1993) 13244-13253.

[10]. F. Wu, P. Bellon, A. J. Melmed, T. Lusby, Acta Mater. 49 (2001) 453-461.

[11]. J. Xu., G. S. Collins, L. S. J. Peng, M. Atzmon, Acta Mater. 47 (1999) 1241-1253.

[12]. M. Sherif El-Eskandarany, M. Matsushitaa, A. Inoue., J. Alloys. Comp. 329 (2001) 239–252.

[13]. T. Tsurui, A.P. Tsai, A. Inoue, T. Masumoto, J. Alloys. Compo. 218 (1995) L7-L10.

[14]. B.L. Huang, R.J. Perez, E.J. Lavernia, M. J. Luton, Nanostruc. Mater. 7 (1996) 67-79.

[15]. G. Cardellini, M. Mazzone, Vittori Ntisari**,** Acta Mater. 44 (1996) 1511-1517.

[16]. A. Inoue, Bulk Amorphous Alloys–Preparation and Fundamental Characteristics, Materials Science Foundation 4 (Trans Tech, Netherlands, 1998) p.1.

[17]. P. Ramchandra Rao, Z. Metallk. 71 (1980) 172-177

[18]. T Egami, Mater. Sci. Eng. A 226-228 (1997) 261-267.

[19]. A.R. Yavari, P. J. Desre, Mater. Sci. Eng. A 134 (1991) 1315-1322.

[20]. J. Latuch T. Kulik, H. Dimitrov., Mater. Sci. Eng. A 375–377 (2004) 956-960.

[21]. L. Shaw, M. Zawrah, J. Villegas, H. Luo, D. Miracle, Metall. Mater. Trans. A 34A (2003) 159-170.

[22]. C. C. Koch, Nanostructred Mater. 9 (1997) 13-22.

[23]. B.D. Cullity, Elements of X-ray Diffraction, 2nd Edition, Addison Wesley, (Reading, MA, 1978) p.350.

[24]. T.H. Keijser, J.I. Langford, E.J. Mittemeijer, A.B.P. Vogels, J. Appl. Cryst., 15 (1982) 308-314.

[25]. S.K. Pabi, D. Das, T.K. Mahapatra, I. Manna, Acta Mater. 46 (1998) 3501 -3510.

[26]. D. Das, P.P. Chatterjee, I. Manna, S.K. Pabi, Scripta Metall. Mater. 41 (1999) 861-66.

[27]. M.K. Datta, S.K. Pabi, B.S. Murty, J. Appl. Phys. 87 (2000) 8393 – 8400.

[28]. N. Das, G.K. Dey, B.S. Murty, S.K. Pabi, Pramana – J. of Phys. 65 (2005) 831-840.

[29]. N. Das, M.Tech Thesis, IIT, Kharagpur, (2005).

[30]. J. Eckert, in Nanostructured Materials -Processing, Properties and Potential Applications, edited by C.C. Koch (Noyes, New York, 2002), p. 432.

[31]. T. Benameur, A. Inoue, and T. Masumoto, Mater. Trans. JIM 35 (1994) 451-457.

[32]. T. Benameur, A. Inoue, and T. Masumoto, Nanostructed Mater. 4 (1994) 303-322.

[33]. M. Seidel, J. Eckert, H.D. Bauer, L. Schultz, *in* Grain Size and Mechanical Properties – Fundamentals and Applications, edited by M.A. Otooni, R.W. Armstrong, N.J. Grant, K. Ishizaki (Mater. Res. Soc. Symp. Proc., Materials Research Society, Warrendale, PA 1995) p. 239.

[34]. Smithells Metals reference Book. 7th Edition. Edited by E.A. Brandes and G.B. Brook, pp 4-41, 4-42.

[35]. R. B. Schwarz, Y. He, Mater. Sci. Forum 235-238(1997)231-240.

[36]. A. Inoue, Prog. Mater. Sci. 43(1998)365-520.

Figure Captions

Fig. 1 SEM micrographs of $Al_{94.5}Cr_3Co_{1.5}Ce_1$ composition after MA for (a) 5 h and (b) 30 h.

Fig. 2 (a) XRD patterns of $Al_{94.5}Cr_3Co_{1.5}Ce_1$ composition at different instances of MA. (b) Enlarged view of the pattern for 60 h milled sample.

Fig. 3 Variation of crystallite size of Al with milling time of $Al_{94.5}Cr_3Co_{1.5}Ce_1$ alloy. Data compared with that of $Al_{88}Ni_6Ti_6$ and $Al_{60}Ni_{20}Ti_{20}$ alloys, reported in [28] and calculated from [29], respectively.

Fig. 4 Transmission electron micrograph of alloy $Al_{94.5}Cr_3Co_{1.5}Ce_1$ after 60 h of MA. The diffraction pattern in the inset from the encircled area of the micrograph shows diffused ring from amorphous phase and spotty pattern from nanocrystalline Al phase.

Fig. 5 Lattice microstrain vs. milling time for $Al_{94.5}Cr_3Co_{1.5}Ce_1$, $Al_{88}Ni_6Ti_6$ and $Al_{60}Ni_{20}Ti_{20}$ alloys (see text).

Fig. 6 Variation of lattice parameter of Al in $Al_{94.5}Cr_3Co_{1.5}Ce_1$ alloy with milling time, compared with that of $Al_{88}Ni_6Ti_6$ alloy reported in [28] and $Al_{60}Ni_{20}Ti_{20}$ alloy [29] milled under identical condition [see text].

Fig. 7 DSC thermogram of $Al_{94.5}Cr_3Co_{1.5}Ce_1$ alloy measured in He atmosphere at a heating rate 5ºC min^{-1} following mechanical alloying for 60 h showing strongly exothermic peaks approximately at 148ºC and 187ºC.

Fig. 8 XRD pattern of 60 h milled sample, after annealing at 200ºC for 2 h.

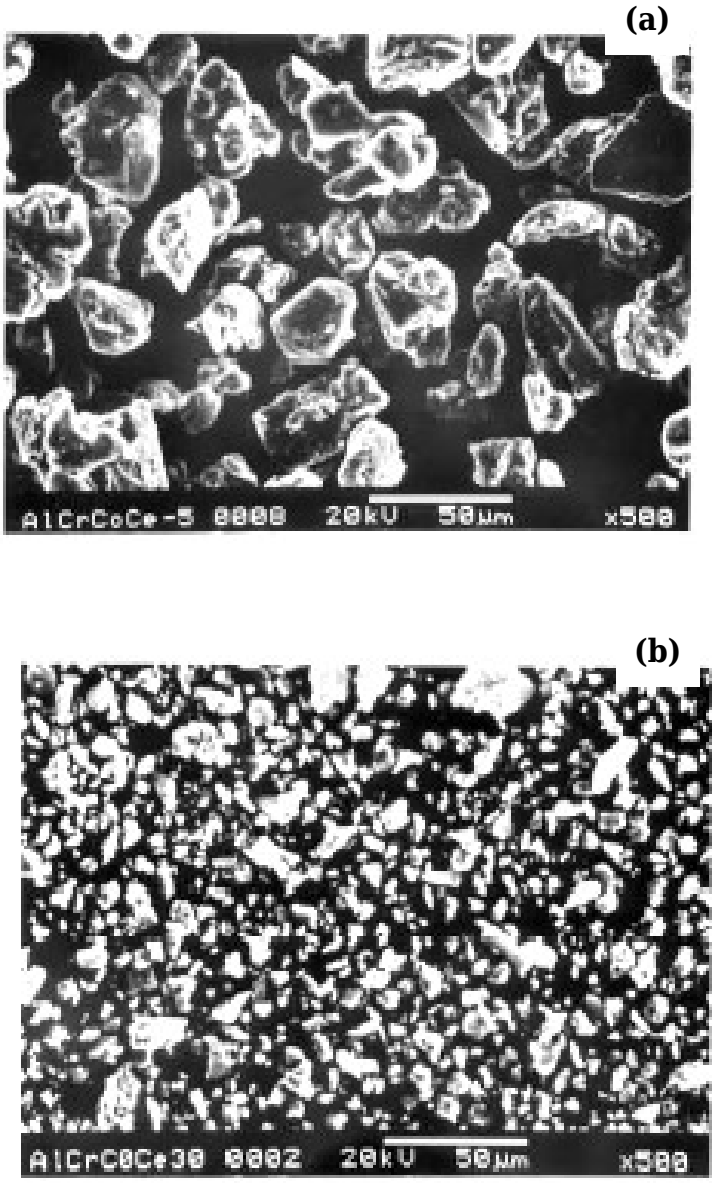

Fig. 1 SEM micrographs of $Al_{94.5}Cr_3Co_{1.5}Ce_1$ composition after MA for (a) 5 h and
(b) 30 h.

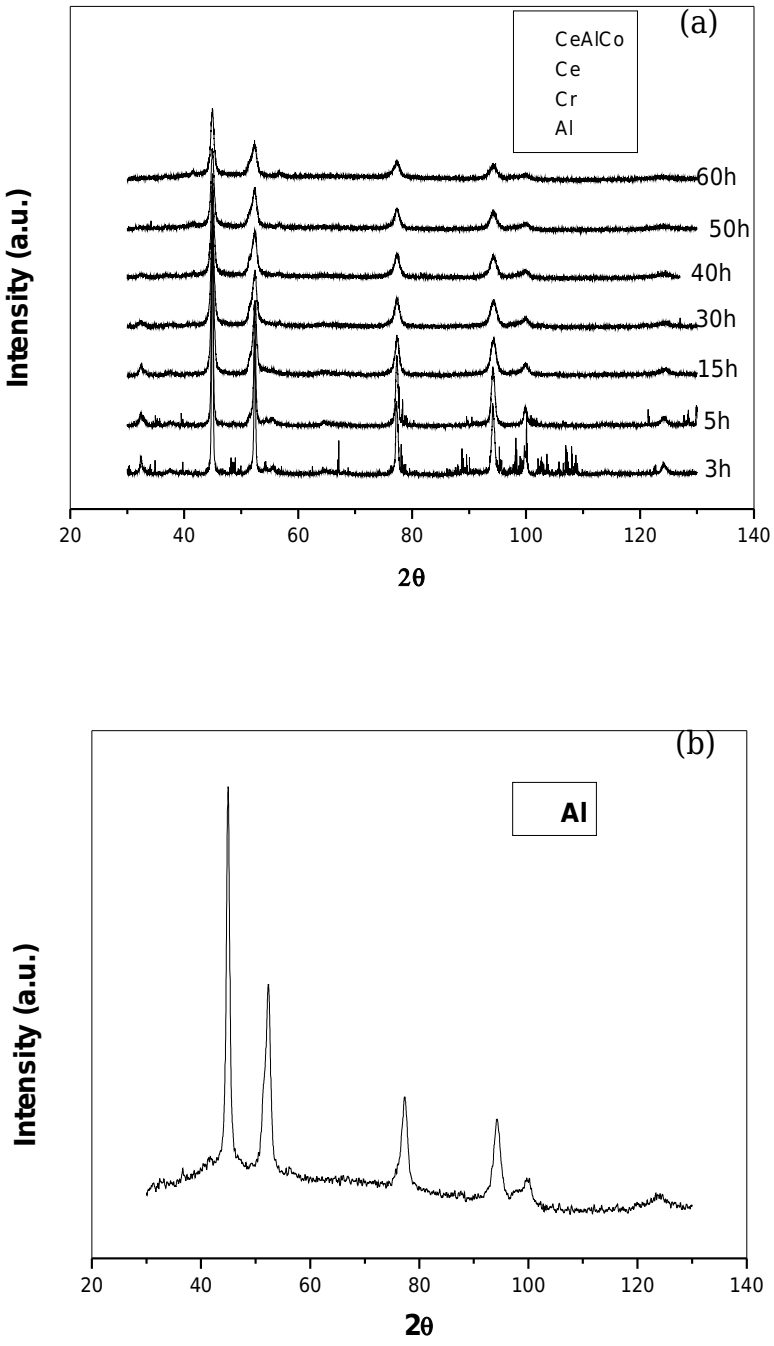

Fig. 2 (a) XRD patterns of $Al_{94.5}Cr_3Co_{1.5}Ce_1$ composition at different instances of MA.
(b) Enlarged view of the pattern for 60 h milled sample.

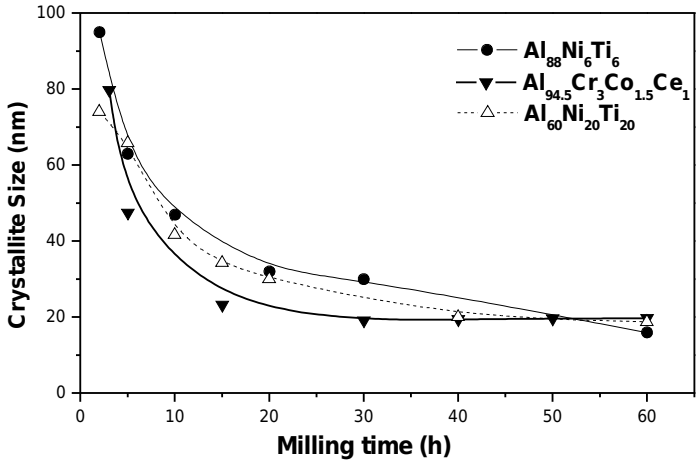

Fig. 3 Variation of crystallite size of Al with milling time of $Al_{94.5}Cr_3Co_{1.5}Ce_1$ alloy. Data compared with that of $Al_{88}Ni_6Ti_6$ and $Al_{60}Ni_{20}Ti_{20}$ alloys, reported in [28] and calculated from [29], respectively.

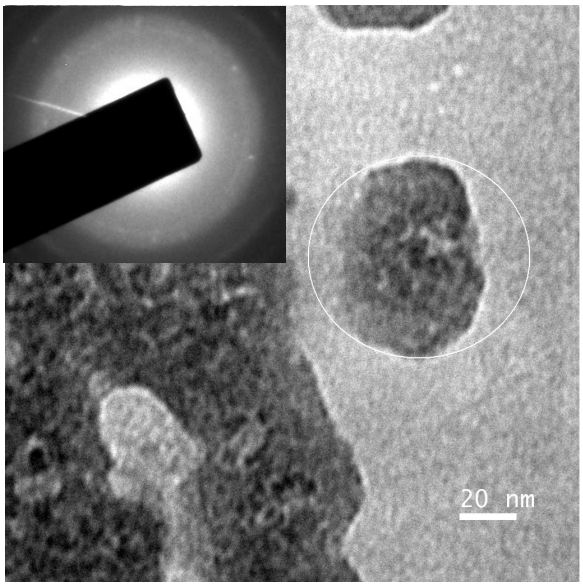

Fig. 4 Transmission electron micrograph of alloy $Al_{94.5}Cr_3Co_{1.5}Ce_1$ after 60 h of MA. The diffraction pattern in the inset from the encircled area of the micrograph shows diffused ring from amorphous phase and spotty pattern from nanocrystalline Al phase.

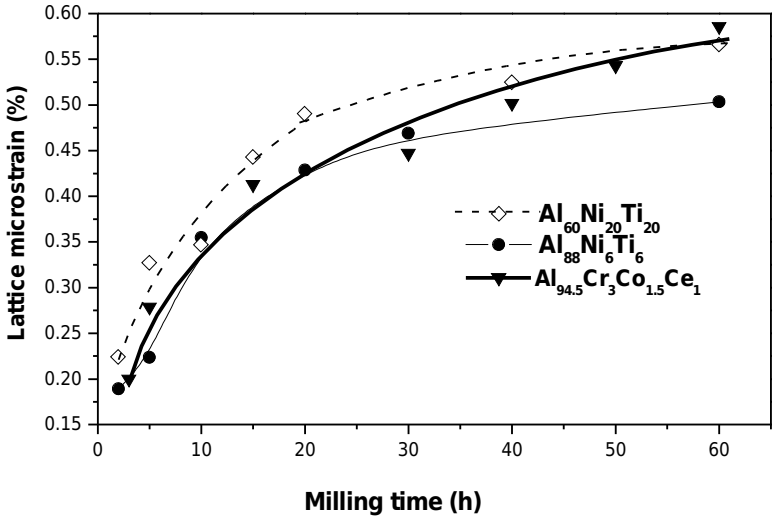

Fig. 5 Lattice microstrain vs. milling time for $Al_{94.5}Cr_3Co_{1.5}Ce_1$, $Al_{88}Ni_6Ti_6$ and $Al_{60}Ni_{20}Ti_{20}$ alloys (see text).

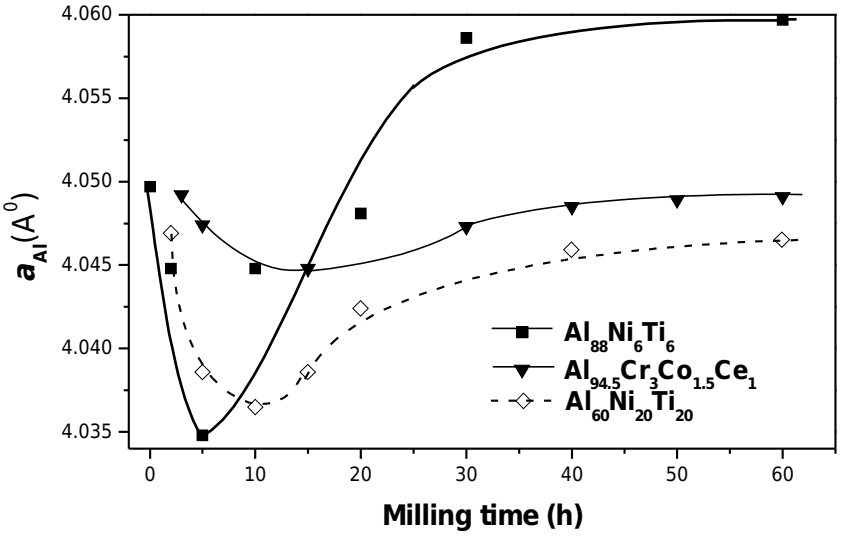

Fig. 6 Variation of lattice parameter of Al in $Al_{94.5}Cr_3Co_{1.5}Ce_1$ alloy with milling time, compared with that of $Al_{88}Ni_6Ti_6$ alloy reported in [28] and $Al_{60}Ni_{20}Ti_{20}$ alloy [29] milled under identical condition [see text].

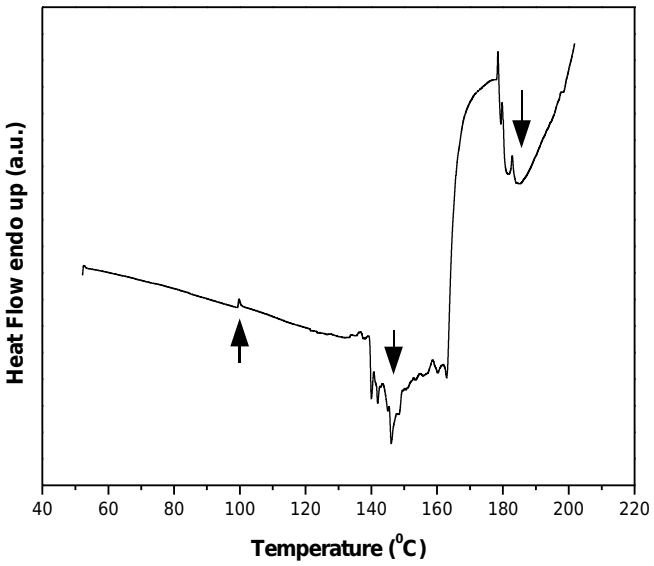

Fig. 7 DSC thermogram of $Al_{94.5}Cr_3Co_{1.5}Ce_1$ alloy measured in He atmosphere at a heating rate 5ºC min^{-1} following mechanical alloying for 60 h showing strongly exothermic peaks approximately at 148ºC and 187ºC.

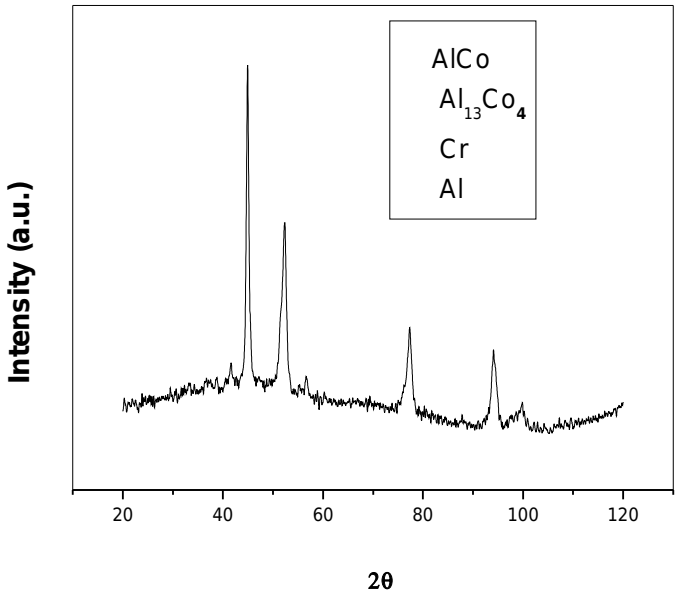

Fig. 8 XRD pattern of 60 h milled sample, after annealing at 200ºC for 2 h.